Displacements, damage measures and response spectra obtained from a synthetic accelerogram processed by causal and acausal Butterworth filters

Pelin Gundes Bakir[†]

Department of Civil Engineering, Istanbul Technical University, Pembegul sok. Pelin apt.
No:20 D:5 Suadiye Istanbul, Turkey

Richard J. Vaccaro[‡]

Department of Electrical and Computer Engineering, University of Rhode Island,
4 East Alumni Ave. Kingston, RI 02881, USA

Abstract. The aim of this study is to investigate the reliability of strong motion records processed by causal and acausal Butterworth filters in comparison to the results obtained from a synthetic accelerogram. For this purpose, the fault parallel component of the Bolu record of the Duzce earthquake is modeled with a sum of exponentially damped sinusoidal components. Noise-free velocities and displacements are then obtained by analytically integrating the synthetic acceleration model. The analytical velocity and displacement signals are used as a standard with which to judge the validity of the signals obtained by filtering with causal and acausal filters and numerically integrating the acceleration model. The results show that the acausal filters are clearly preferable to the causal filters due to the fact that the response spectra obtained from the acausal filters match the spectra obtained from the simulated accelerogram better than that obtained by causal filters. The response spectra are independent from the order of the filters and from the method of integration (whether analytical integration after a spline fit to the synthetic accelerogram or the trapezoidal rule). The response spectra are sensitive to the chosen corner frequency of both the causal and the acausal filters and also to the inclusion of the pads. Accurate prediction of the static residual displacement (SRD) is very important for structures traversing faults in the near-fault regions. The greatest adverse effect of the high pass filters is their removal of the SRD. However, the noise-free displacements obtained by double integrating the synthetic accelerogram analytically preserve the SRD. It is thus apparent that conventional high pass filters should not be used for processing near-fault strong-motion records although they can be reliably used for far-fault records if applied acausally. The ground motion parameters such as ARIAS intensity, HUSID plots, Housner spectral intensity and the duration of strong-motion are found to be insensitive to the causality of filters.

Keywords: response spectra; signal processing; butterworth filters; strong-motion accelerograms; static residual displacement; signal to noise ratios; long period ground motion; synthetic accelerograms; causal/ acausal filters; ARIAS intensity; HUSID plots; Housner spectral intensity; strong-motion duration.

† Associate Professor, Corresponding author, E-mail: gundes@itu.edu.tr
‡ Professor, E-mail: vaccaro@ele.uri.edu

1. Introduction

Signal processing of earthquake records is the first and most important step of any type of earthquake engineering analysis. Despite its importance however, the processing procedures adopted by strong ground motion processing centers are still not standardized. Currently, the majority of the processing centers use Butterworth filters for processing strong-motion records. Butterworth filters like any other filters can be classified into two with respect to their phase characteristics. The first are the causal filters whose output depend only on past and present inputs. However, causal filters distort the phase of the input signal components with frequencies in the passband. The second type of filters are the acausal filters which have no phase distortions. One way to prevent any phase distortions is to make the frequency response of the filter real and nonnegative, in other words, to design the filter with a zero phase characteristic. For non-real-time processing of real-valued input signals of finite length, zero-phase filtering can be very simply implemented if the causality requirement is relaxed. To achieve this zero phase shift, the finite length input data is processed through a causal real-coefficient filter whose output is then time-reversed and processed by the same filter again. The output vector is reversed to obtain the desired zero phase shift data. A sufficient number of zeros must be added to the input data to accommodate the filter response. This procedure is defined as acausal filtering (Kanasewich 1981, Mitra 2001). It should be stated that the terms causality and acausality do not solely pertain to Butterworth filters. The disadvantage of the acausal Butterworth filters is that padding may introduce filter transients at the beginning of the records.

One of the aims of this study is to investigate which type of filter application will be more appropriate for processing strong-motion records. Boore and Akkar (2003) have compared the displacement and response spectra obtained from causal and acausal filters. The present study on the other hand, compares the displacement and response spectra obtained from causal and acausal filters to those obtained from an unfiltered noise-free synthetic accelerogram. For this purpose, a real earthquake accelerogram is modeled with a sum of exponentially damped sinusoidal components. The acceleration signal modeled is the fault parallel component of the Bolu record of the magnitude $M_w = 7.2$ November 12, 1999 Duzce earthquake in Turkey. The Duzce earthquake produced very severe strong ground motions and the Bolu record is a high-quality digital recording obtained close to the source of the Duzce earthquake. The Bolu record is used as recorded and it is not rotated. The fault-slip and ground-shaking demands on the Bolu viaduct are discussed comprehensively by Park *et al.* (2004) and by Priestley and Calvi (2002). A general review on the 1999 Kocaeli and Duzce earthquakes can be found in other papers of the authors (Bakir and Boduroglu 2002a,b, Bakir 2004, Bakir and Boduroglu 2004). When the Duzce earthquake hit the city of Duzce in 1999, Bolu was in the forward directivity direction of the ruptured segment of the fault. Forward directivity occurs when the rupture front propagates toward the site and the direction of the fault slip is aligned with the site. The Bolu record shows a strong velocity pulse in the N-S direction and increased spectral values at long periods (periods greater than 2 seconds). These large velocity pulses may occur either due to directivity or fling. Fling is associated with permanent ground displacements due to surface fault rupture. Whereas forward directivity produces two sided velocity pulses, fling step is a result of a permanent ground displacement that generates one sided velocity pulses. Fling step is observed as a discrete step in a displacement time history that occurs with strike slip earthquakes (Bray and Rodriguez-Marek 2004, Somerville *et al.* 1997). The acceleration signal model is explained in the following section.

2. Acceleration signal model

Zeroth order correction is the removal of the mean of the pre-event memory from the whole digital accelerogram (Boore *et al.* 2002). An oscillatory signal such as the Bolu record, after zeroth order correction, can be modeled as a sum of exponentially damped sinusoids as follows:

$$a(t) = \sum_{i=1}^{q} e^{-\delta_i t} [\alpha_i'' \cos(\omega_i t) + \beta_i'' \sin(\omega_i t)] \tag{1}$$

where α'', β'' are amplitudes, δ_i are damping factors, and ω_i are frequencies.

The model in Eq. (1) is actually for the noise-free signal. A measured accelerogram will contain an underlying signal of the form (1) plus additive noise. By modeling a measured accelerogram with a limited number of components (the number q in (1)), the model in (1) will be a good approximation to the underlying noise-free acceleration signal. The signal in (1) has the form of an impulse response of a linear, time-invariant (LTI), continuous-time system of order $2q$ (Jackson 1991). If $a(t)$ is sampled, the resulting sequence is the impulse response of a discrete-time LTI system of order $2q$. It is possible to calculate a discrete-time state-space model from a given, discrete time impulse response using, for example, the algorithm in Vaccaro (1983), Mulholland *et al.* (1986). The signal parameters in (1) may be obtained directly from the discrete-time state-space model using formulas derived in Vaccaro (2005), which is available from the authors. For example, the N-S component of the Bolu record was modeled with $q = 175$ in (1). Fig. 1(a) shows the signal $a(t)$ from (1) and Fig. 1(b) shows the Bolu data record. They are indistinguishable on that plot; Fig. 1(c) shows the difference between the recorded accelerogram and the signal $a(t)$. As apparent from the figure, the model provides a good fit to the data record. For the purpose of this paper, $a(t)$ in (1) is an analytical expression for a realistic earthquake accelerogram. The signal $a(t)$ may be twice integrated analytically to obtain noise-free velocity and displacement signals.
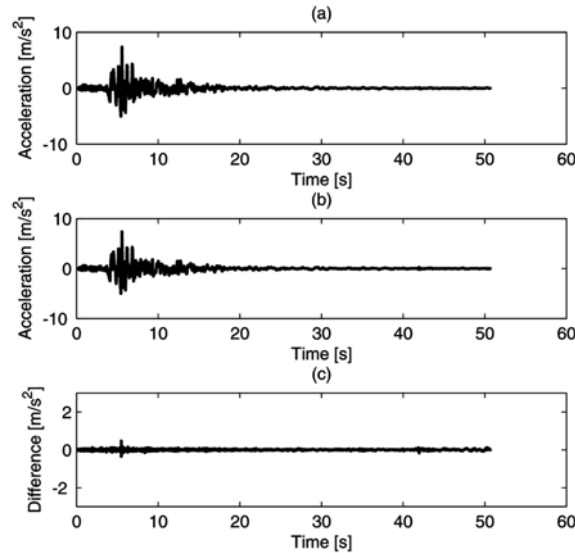

Fig. 1 (a) The analytical accelerogram obtained from state space model, (b) the Bolu record, and (c) the difference between the recorded and the simulated accelerograms

When the signal in (1) is twice integrated, the resulting velocity and displacement signals have the same form as in (1); they are sums of exponentially damped sinusoids. The frequencies and damping factors for velocity and displacement are the same as for the acceleration signal. Only the amplitude parameters differ for the three signals. The analytical velocity and displacement signals are given below:

$$v(t) = \sum_{i=1}^{q} e^{-\delta_i t} [\alpha_i' \cos(\omega_i t) + \beta_i' \sin(\omega_i t)] \tag{2}$$

$$d(t) = \sum_{i=1}^{q} e^{-\delta_i t} [\alpha_i \cos(\omega_i t) + \beta_i \sin(\omega_i t)] + c \tag{3}$$

where the constant c in (3) is chosen to make $d(0) = 0$. Given the parameters of an acceleration signal, the amplitude parameters of the velocity and displacement signals may be calculated as follows. Define

$$s_i = -\delta_i + j\omega_i \tag{4}$$

$$A_i = \alpha_i'' - j\beta_i'' \tag{5}$$

Then the amplitudes of the velocity signal are given by:

$$\alpha_i' = real\left(\frac{A_i}{s_i}\right) \tag{6}$$

$$\beta_i' = -imag\left(\frac{A_i}{s_i}\right) \tag{7}$$
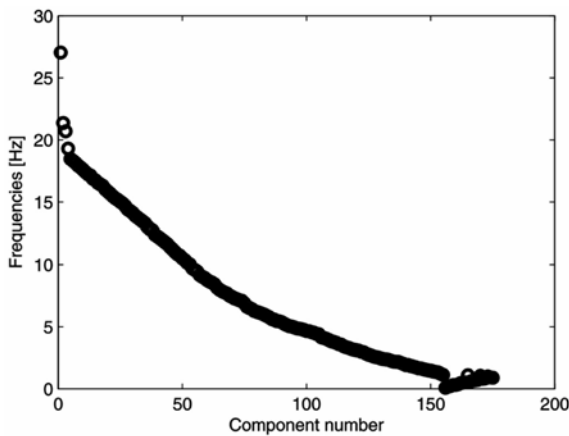

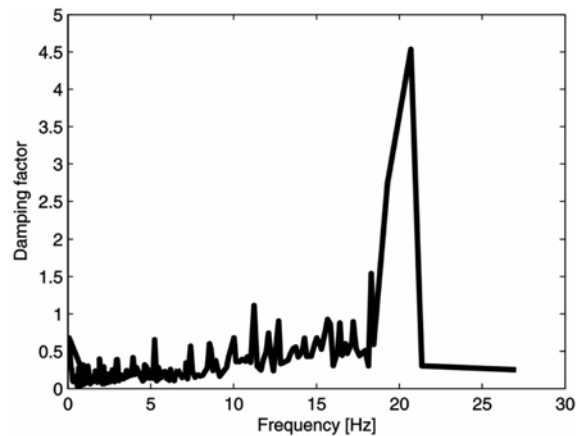Fig. 2 The frequencies for each component of the model
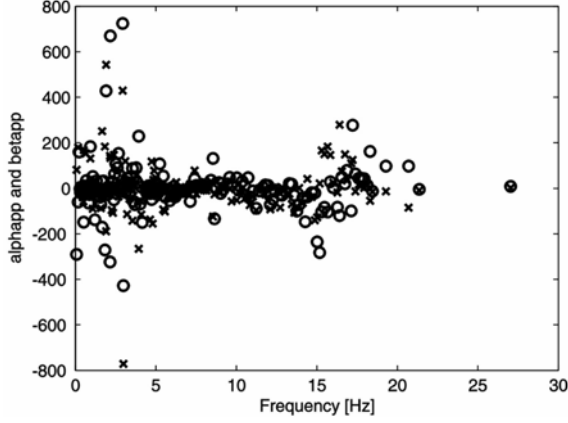
Fig. 3 The damping factors versus frequency

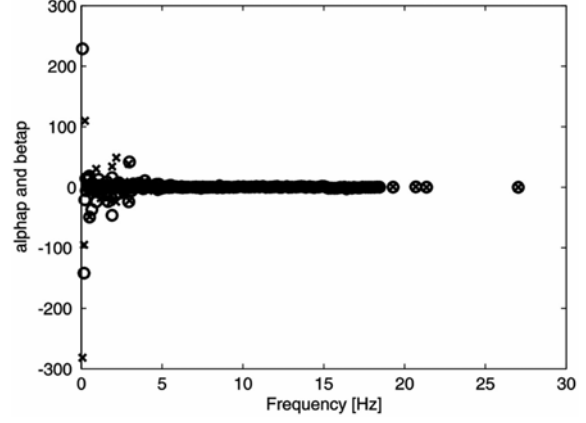Fig. 4 Parameters α'' (denoted as o) and β'' (denoted as x) for the simulated acceleration signal

Fig. 5 Parameters α' (denoted as o) and β' (denoted as x) for the simulated velocity signal
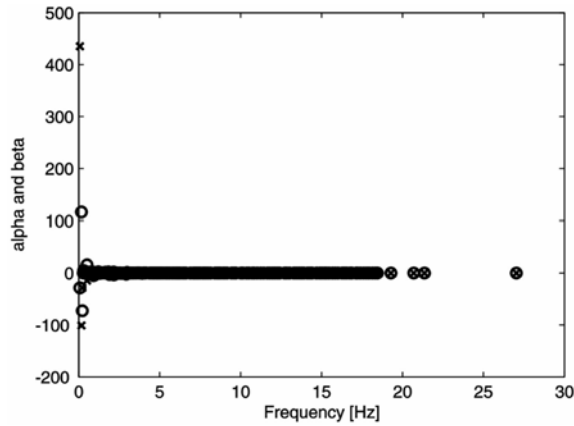

Fig. 6 Parameters α (denoted as o) and β (denoted as x) for the simulated displacement signal

and the amplitudes of the displacement signal are given by:

$$\alpha_i = real\left(\frac{A_i}{s_i^2}\right) \tag{8}$$

$$\beta_i = -imag\left(\frac{A_i}{s_i^2}\right) \tag{9}$$

The frequencies and damping factors for modeling Bolu record are shown in Figs. 2 and 3, whereas the amplitude parameters for the acceleration, velocity and displacement are shown in Figs. 4, 5 and 6 respectively. The actual values for the parameters, damping factors and frequencies to obtain the simulated accelerogram, and the noise-free velocity and displacement can be obtained from the authors.

In the remainder of this paper we compare different conventional methods of processing $a(t)$ and compare results with the noise-free velocity and displacement.
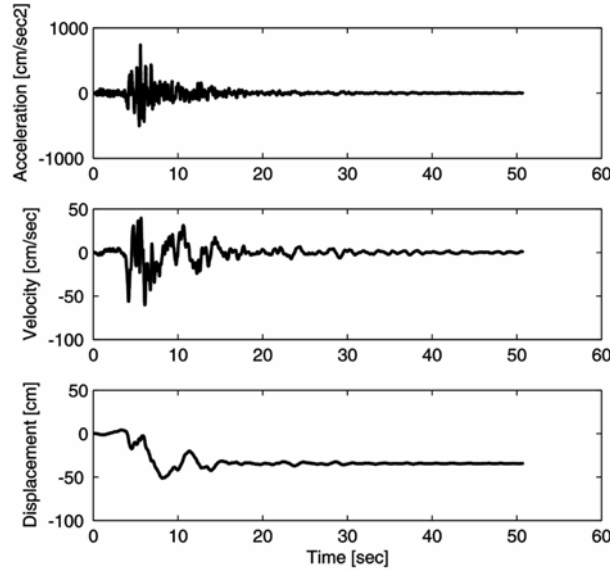
Fig. 7 The noise-free simulated accelerogram and the noise-free velocity and displacement time histories obtained by analytically integrating the acceleration model

3. Signal processing procedures for strong ground motions and comparison with the analytical model

Fig. 7 shows the simulated accelerogram and the noise-free velocity and displacement time histories obtained by analytical integration.

MATLAB (2005) subroutines are developed for all the data processing procedures used in this study. Data processing for strong ground motions starts with the zeroth order correction. In digital accelerograms, a pre-event memory of the signal is often available, and therefore the mean of this pre-event memory is removed from the whole record. In records obtained from analog accelerographs, a pre-event memory of the signal is not available, and the mean of the whole record is removed from the signal (Boore *et al.* 2002). The second step is to use tapers before and after zero pads to prevent ringing in the integrated displacements. The remainder of the signal processing steps for ground motions are explained in the following subsections:

3.1 Zero pads for acausal filters

Acausal filters need zero padding before and after the records to obtain zero phase shifts (Boore and Bommer 2005). The pad length is calculated by the empirical formula given by Converse and Brady (1992) as follows:

$$t_p = 1.5 \frac{n_{roll}}{f_c} \tag{10}$$

where t_p is the pad length in seconds, n_{roll} is the roll-off parameter which is equal to half of the order of the Butterworth filter (Stephens and Boore 2004) and f_c is the corner frequency. Boore
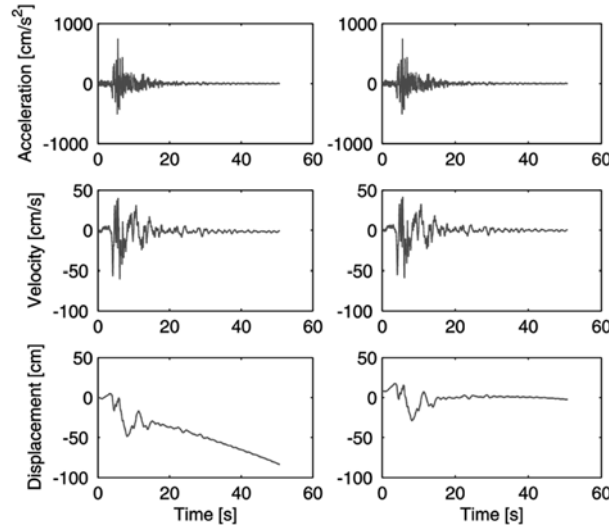
Fig. 8 Analytical noise-free accelerogram numerically integrated without pads (left-hand side) and integrated with pads (right-hand side) by a causal low pass filter with corner frequency of 20 Hz and a high pass acausal Butterworth filter with a corner frequency of 0.025 Hz

(2005a) has stated that if pads are not appended to the acceleration data, low-frequency noise will be reintroduced into the velocity and displacements as well as the response and Fourier spectra. Fig. 8 shows the influence of padding the acceleration data for the simulated accelerogram and displacements after numerical integration. The displacement time history obtained from pad stripped data is clearly unrealistic for a record of 17.6 kilometers to the fault. This figure clearly shows that the padded sections appended at the beginning and at the end of the acceleration data should be retained for subsequent processing.
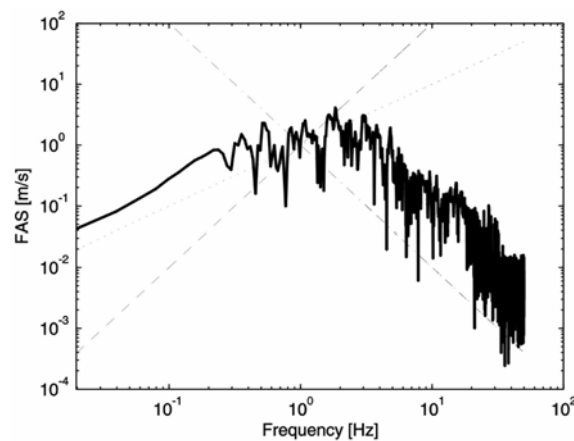

Fig. 9 Fourier Amplitude Spectrum of the analytical accelerogram: signal (solid line), f^2 (dashed line), f (dashed line), $1/f^2$ (dashed-dotted line). The high pass filter corner frequency chosen from this FAS is 0.025 Hz.

3.2 Fourier amplitude spectrum

The frequency content of the ground motion can be examined by transforming the acceleration data from the time domain to the frequency domain through a Fourier transform. If causal or acausal filters are used for digital signal processing of strong-motion data, it is essential to obtain the FAS of the signal in order to determine the corner frequency of the Butterworth filter. For this purpose, noise with standard deviation of the order of a thousandth of g is added to the simulated accelerogram. Fig. 9 shows the FAS of the noisy simulated accelerogram. The corner frequency for the high pass filter is selected based on the f^2 source model of Brune (1970, 1971), Boore (2005b) and it is 0.025 Hz for this case. The figure also indicates that most of the energy in the synthetic accelerogram is between the frequencies of 0.1 to 15 Hz, and the largest amplitude is at a frequency of 1.8 Hz.

3.3 Low pass Butterworth filters

The purpose of a low pass filter is to remove the part of the signal that is judged to be heavily contaminated by high-frequency noise that is often observed in strong-motion records. A low-pass filter passes low-frequency components in the signal with minimal distortion and attenuates the high-frequency components. The so-called cutoff or corner frequency divides the pass band and the stop band. A low pass causal Butterworth filter is an all pole filter with a squared magnitude response given by:

$$|H(\omega)|^2 = \frac{1}{1 + \left(\dfrac{\omega}{\omega_c}\right)^{2n}} \tag{11}$$

where n is the order of the filter (number of poles in the system function) and ω_c is the cut off frequency of the Butterworth filter which is the frequency where the magnitude of the causal filter $|H(\omega_c)|$ is $1/\sqrt{2}$ regardless of the order of the filter. $|H(\omega_c)|$ takes the value of 0.5 for acausal filters. The mathematical reasoning behind this can be explained as follows: If we let $H_c(\omega)$ be the frequency response of the causal Butterworth filter given by Eq. (11), this filter has unity gain at frequency $\omega = 0$. The cutoff frequency ω_c is the frequency at which the power of the filter ouput is half the power of the filter input, i.e., $|H_c(\omega_c)|^2 = 1/2$. The frequency response of an acausal Butterworth filter $H_a(\omega)$ is given by:

$$H_a(\omega) = H_c(\omega)H_c(-\omega) \tag{12}$$

The previous equation shows that $|H_a(\omega_c)| = 1/2$. The frequency response of a Butterworth filter
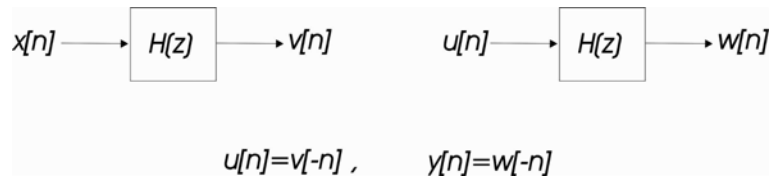

Fig. 10 Implementation of a zero-phase filtering scheme (Mitra 2001)

decreases monotonically with increasing frequency, and as the filter order increases, the transition band becomes narrower. The low pass filters can be applied either causally or acausally. The implementation of a zero-phase filtering scheme is shown in Fig. 10.

3.4 High pass acausal Butterworth filters

High pass Butterworth filters are filters which pass all the frequencies above the corner frequency and block all the frequencies below the corner frequency. High pass filters can also be applied either causally or acausally. If Figs. 7 and 8 are compared, it is apparent that the main effect of high pass filters is to remove the static residual displacement (SRD). This can be explained as follows: To preserve the SRD at the end of the record, the velocity should have non-zero mean. This can only be achieved if the *d.c.* component of the velocity Fourier transform is non-zero. However, with high pass filtering, the *d.c.* component is removed from the velocity signal. Since the displacement starts at zero, and velocity has zero mean after high pass filtering, the consequence is the removal of the SRD. The majority of the damage observed at the overpasses and bridges in the 1999 Kocaeli and Duzce earthquakes were due to the displacement field caused by the tectonic ground movement (Park *et al.* 2004, Priestley and Calvi 2002). That is the main reason why SRD has gained significant attention among the engineering community over the past years. Currently, baseline correction methods are used to recover SRD. These correction methods are sensitive to the processing parameters. The SRD obtained from these methods is largely dependent on the parameters chosen for the models. The end user of the methods may never be sure of the real value of the SRD unless there is a global positioning system (GPS) sensor co-located with the fault, the displacement field is determined from satellite interferometry or from classical geodetic field
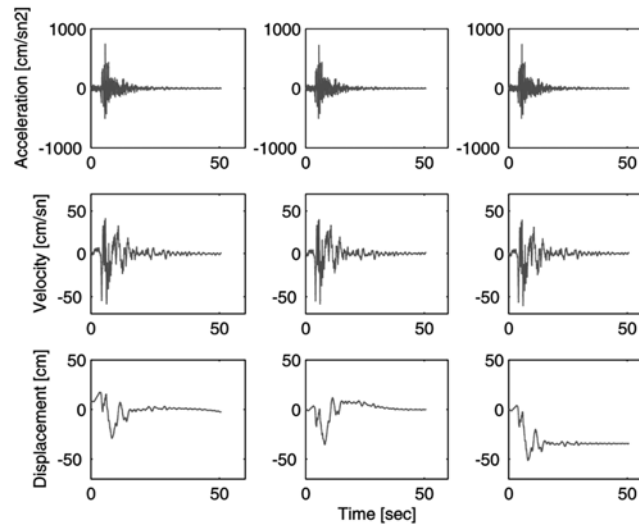

Fig. 11 The influence of causality of the filter on the acceleration, velocity and displacement time history, acausal filters (left-hand side), causal filters (middle column), simulated noise-free acceleration, velocity and displacement (right-hand side). The high pass corner frequency of the Butterworth filter is 0.025 Hz, the low pass corner frequency of the Butterworth filter is 20 Hz and the order of the filter is 2. The leading and trailing pads used in acausally filtered data are stripped off for illustration purposes in the figure.
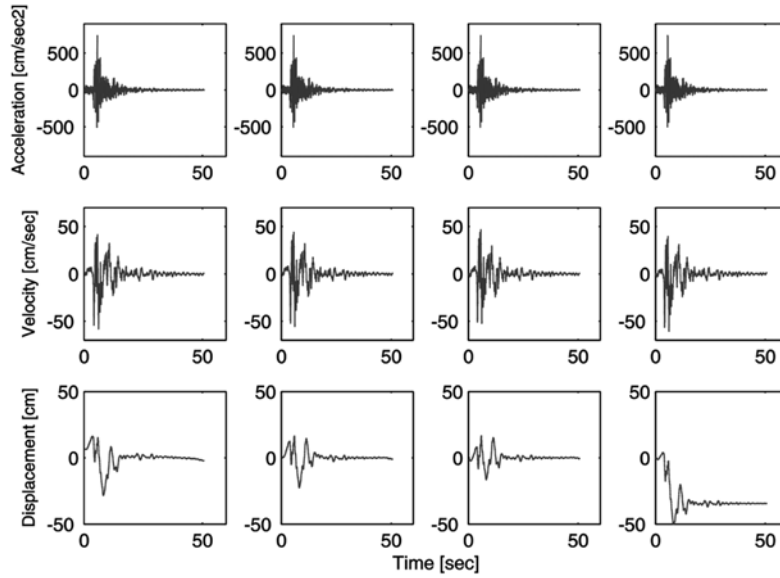
Fig. 12 Displacement and velocity time history obtained by applying acausal high pass Butterworth filters with different corner frequencies on the noisy simulated accelerogram (from left column to the right: f_c = 0.03 Hz, f_c = 0.06 Hz, f_c = 0.1 Hz), the low pass filter corner frequency is 20 Hz and the order of the filter is 2. Superimposed on the figure are the simulated noise-free accelerogram, velocity and displacement (right-hand side).
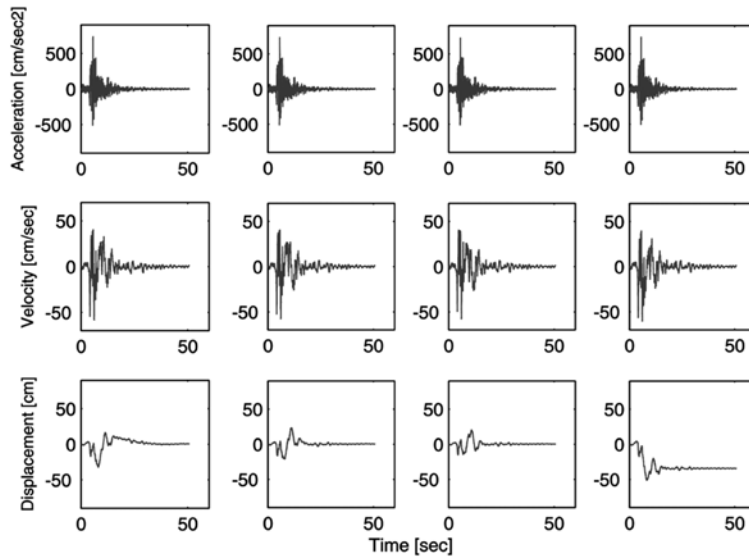

Fig. 13 Displacement and velocity time history obtained by applying causal high pass Butterworth filters with different corner frequencies on the noisy simulated accelerogram (from left column to the right: f_c = 0.03 Hz, f_c = 0.06 Hz, f_c = 0.1 Hz), the low pass filter corner frequency is 20 Hz and the order of the filter is 2. Superimposed on the figure are the simulated noise-free accelerogram, velocity and displacement (right-hand side).
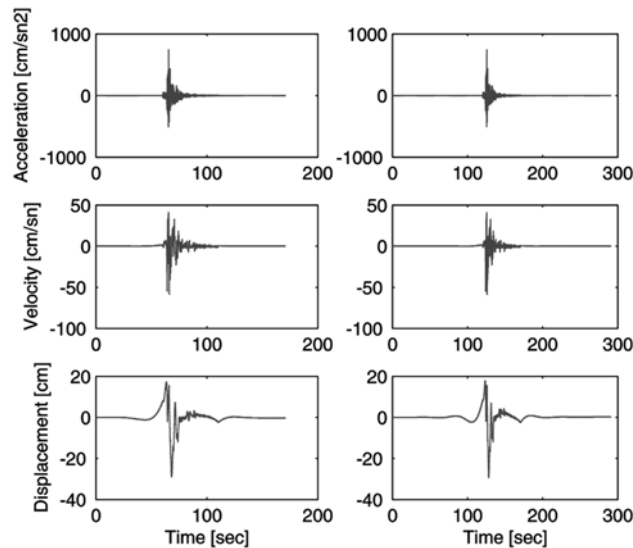
Fig. 14 The influence of the order of the filter on the noise-free simulated acceleration, velocity and displacement time history for a filter order of 2 (left-hand side) and 4 (right-hand side). The high pass corner frequency of the acausal Butterworth filter is 0.025 Hz and the low pass corner frequency of the causal Butterworth filter is 20 Hz. The leading and trailing pads used are stripped off for illustration purposes in the figure.

surveying techniques. Fig. 11 shows the influence of the causality of the high pass filters on the acceleration, velocity and displacement time history. The displacements are significantly affected by the causality of the filter and phase shifts are observed in both cases. But what is most striking from the figure is that the data filtered by both causal and acausal filters do not match the theoretically exact velocity and displacements of the model. The difference is especially significant in displacements where the high pass filters, whether causal or acausal, both filter out the SRD.

The response of high-pass Butterworth filters is very much dependent on the choice of filter corner frequency. Fig. 12 shows the noisy simulated accelerogram filtered with high-pass Butterworth filters with different corner frequencies and the noise-free simulated acceleration, velocity and displacements. It is apparent that the displacement waveform and the PGD are substantially affected by the choice of corner frequency. None of the displacement time histories match the theoretically exact displacement time history. The phase shifts in displacements are much more significant for data obtained with causal filters as shown in Fig. 13.

The order of the Butterworth filters is also of concern. If the filter cuts all the frequencies sharply at the corner frequency, then the wave form will be distorted severely. In order to prevent this, a transition zone is necessary between the frequencies blocked and frequencies that pass. This transition is called roll-off and the roll-off parameter is half the order of a Butterworth filter (Converse and Brady 1992, Stephens and Boore 2004). Boore and Bommer (2005) have stated that the higher the order of a Butterworth filter, the more abrupt will be the cut-off. Fig. 14 compares the simulated noise-free accelerogram processed by a filter of order 2 (left-hand side) and order 4 (right-hand side) respectively. It is apparent that doubling the filter order does not cause much difference in the velocity and displacement waveforms as well as the PGV and PGD values.
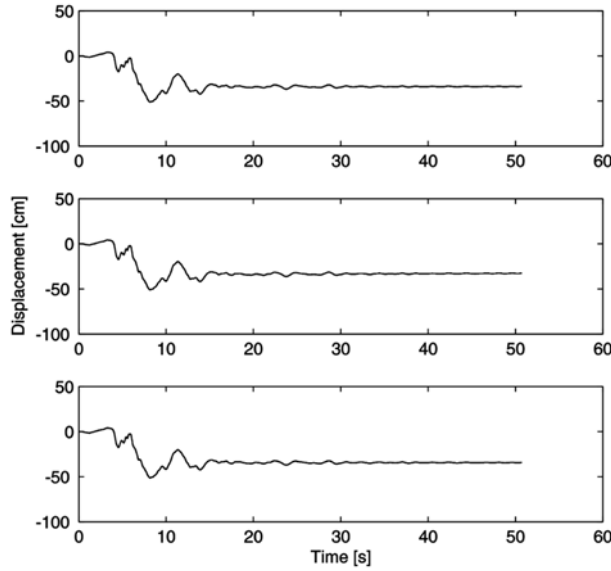
Fig. 15 The displacement time history obtained by double integrating the noise-free simulated accelerogram using trapezoidal rule (top row), spline integration (middle row), and from the noise-free analytical model (bottom row)

3.5 Integration with splines and the trapezoidal rule

Splines are smooth piecewise polynomials that can be used to represent functions over large intervals, where it would be impractical to use a single approximating polynomial. The traditional trapezoidal method used for the integration of the filtered accelerograms is compared with the analytical integration of the splines fit to the synthetic accelerogram. It is apparent from Fig. 15 that the data integrated from the noise-free simulated accelerogram both with the trapezoidal rule and using splines match the noise-free simulated velocities and displacements exactly. Therefore, it can be confidently stated that the effect of the integration method on the displacement time history is insignificant.

4. Strong-ground motion and damage

The damage potential of seismic excitation can not be described by PGA, PGV or PGD alone, but it can better be described by ground-motion parameters such as ARIAS intensity, HUSID diagrams, strong-motion duration, power of the strong-motion and Housner spectral intensity. The ARIAS intensity is a measure of the total energy content of a strong ground motion and is defined by the following equation:

$$I_A = (\pi/2g)\int_0^{t_d} a(t)^2 dt \tag{13}$$

Table 1 Comparison of the seismic damage measures for the unfiltered simulated noise-free accelerogram, the simulated noise-free accelerogram filtered by causal filters and acausal filters

Acceleration signal	PGA [m/sec^2]	PGV [m/sec]	PGD [m]	AI [m^2/sec^3]	Ts [sec]	I_H [m]	Power [1/sec]
AA	7.39	0.604	0.51	3.854	9.76	2.19	0.094
AA causal filter	7.24	0.587	0.35	3.848	9.75	2.18	0.094
AA acausal filter	7.42	0.585	0.29	3.859	9.77	2.19	0.094

Note: 'AA' is the simulated noise-free accelerogram, 'AA causal filter' is the simulated noise-free accelerogram processed by a high pass causal Butterworth filter, 'AA acausal filter' is the simulated noise-free accelerogram processed by an acausal high pass Butterworth filter. The high pass corner frequency for the causal and acausal Butterworth filters are 0.025 Hz. In both cases, the low pass filter is a causal Butterworth filter with a corner frequency of 20 Hz. AI is the ARIAS intensity and I_H is the Housner spectral intensity.

where, I_A is the ARIAS intensity, t_d is the total seismic duration and $a(t)$ is the ground acceleration. The HUSID diagram shows the accumulation of the energy content and is defined as the build-up of Arias intensity as a proportion of the final total. In this study, the Husid diagrams are normalized by the Arias intensity.

The Trifunac and Brady's strong-motion duration (Brady and Trifunac 1975) is defined as the time interval between 5% and 95% of the integral of the square of the ground acceleration.

Housner (1952) defined a measure of the severity of the earthquakes which is essentially the area under the pseudo velocity spectrum between 0.1 and 2.5 s. This measure can be defined as follows:

$$I_H = \int_{0.1}^{2.5} PSV(T,\xi)dT = \frac{1}{2\pi}\int_{0.1}^{2.5} PSA(T,\xi)TdT \qquad (14)$$

Housner spectral intensity is the first moment of area of PSA about the PSA axis, implying that it is larger for ground motions with a significant amount of low-frequency content. Ground motions which have larger magnitude can cause more damage to tall structures (Kiremidjian and Singhal 1996). Table 1 shows several damage measures for the unfiltered, noise-free simulated accelerogram, simulated noise-free accelerogram filtered by causal and acausal filters. It is apparent from the table that both the PGA, PGV as well as PGD are sensitive to the causality of the filters. However, the most sensitive parameter among the three is certainly PGD. The other damage measures are independent of the causality of filters.

The influence of the causality of the filters in comparison to the HUSID plot of the simulated accelerogram is given in Fig. 16. It is apparent that the HUSID plots are independent of the causality of the filters and can be used confidently as a measure of damage irrespective of the processing method.

Fig. 17 shows the HUSID diagram for the simulated noise-free accelerogram in comparison to the simulated noisy accelerogram processed by acausal filters with different corner frequencies. It is apparent that the HUSID diagram is independent of the corner frequency chosen for the acausal filter.
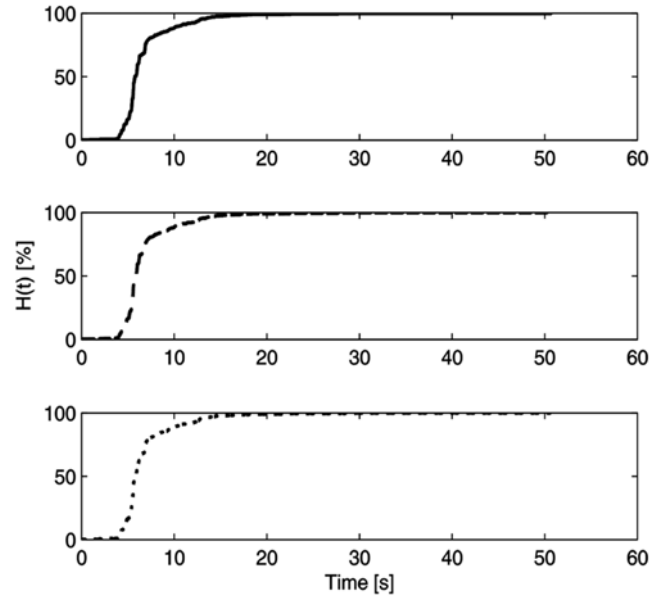
Fig. 16 HUSID diagram of the simulated noise-free accelerogram (dotted line) and the simulated noise-free accelerogram processed by acausal filters (solid line) and causal filters (dashed line)
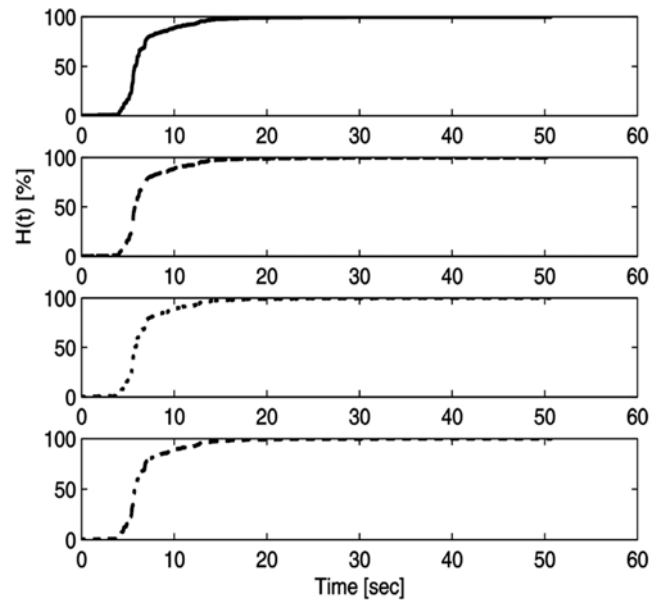

Fig. 17 HUSID diagram of the simulated noise-free accelerogram (dashed-dotted line) and simulated noisy accelerogram processed by causal filters with corner frequencies f_c = 0.03 Hz (solid line), f_c = 0.06 Hz (dashed line) and f_c = 0.1 Hz (dotted line), the low pass filter corner frequency is 20 Hz and the order of the filter is 2.
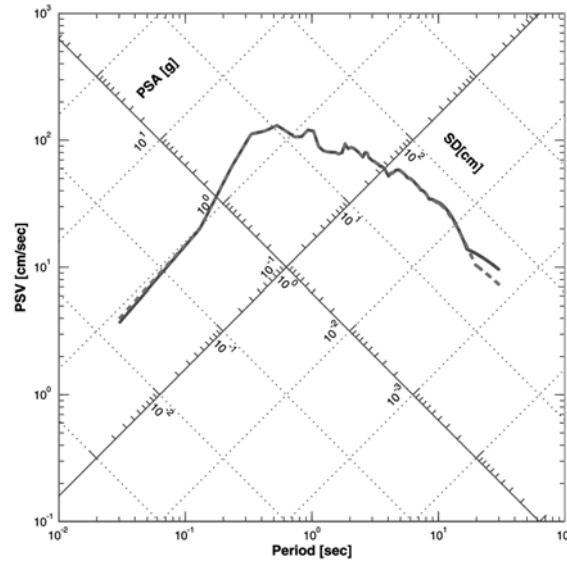
Fig. 18 Response spectra of the simulated noisy accelerogram (solid line) and the unfiltered actual Bolu accelerogram (dashed line)

5. Response spectra

Response spectra are calculated by the piecewise exact method in this study as given in Nigam and Jennings (1968). The PSV, PSA and the SD are related to each other by Eq. (15) (Chopra 2001, Newmark and Hall 1982).

$$PSA\left(\frac{T}{2\pi}\right)^2 = PSV\left(\frac{T}{2\pi}\right) = SD \tag{15}$$

In order to show that the artificial record really does reproduce the characteristics of the Bolu accelerogram, the real and the artificial records should be compared in terms of Arias intensity and response spectra. It should be stated that complete comparison is not possible precisely because the real record is contaminated by noise, and the simulated accelerogram is noise free.

For this purpose, a second version of the artificial record is used, to which 'noise' is added, and the response spectra as well as the Arias intensities of these two records are compared. Fig. 18 shows the response spectra due to the noisy simulated accelerogram and the real unfiltered Bolu accelerogram. The figure shows that the two spectra match each other very closely. The Arias intensity for both the noisy simulated accelerogram and the unfiltered Bolu accelerogram are 3.84. Therefore, it can be concluded that the noisy simulated accelerogram does reproduce the real Bolu accelerogram quite accurately.

6. Implications for engineering structures

Fig. 19 shows the response spectra obtained from the simulated accelerogram processed with filter orders of 2 and 4. The results show that the response spectra obtained are identical for a large
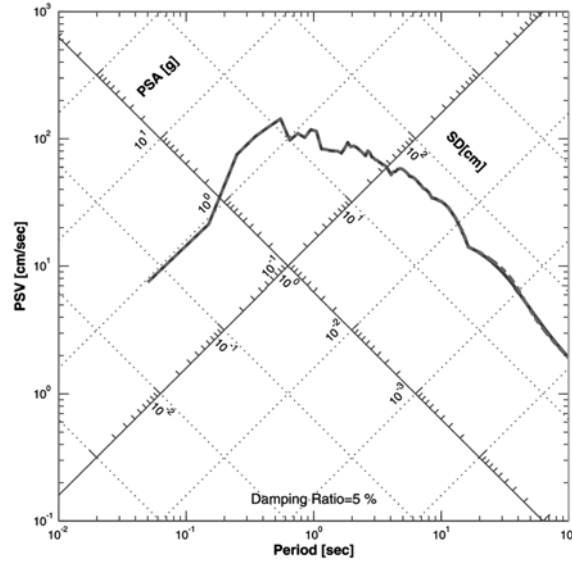
Fig. 19 Response spectra (damping ratio ξ = 5%) obtained from noise-free simulated accelerogram processed with filter orders of 2 (solid line) and 4 (dashed line). The high pass filter corner frequency is 0.025 Hz, the low pass filter corner frequency is 20 Hz and the order of the filter is 2.
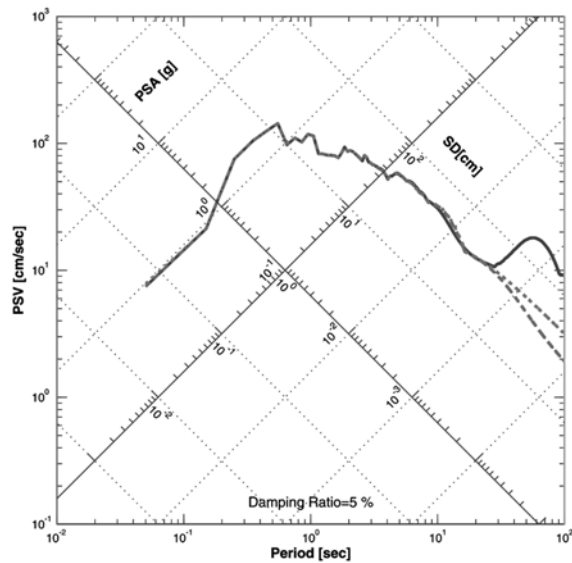

Fig. 20 Response spectra (damping ratio ξ = 5%) obtained from noise-free simulated accelerogram with pads (dashed line), without pads (solid line) and unfiltered simulated noise-free accelerogram (dotted line). A causal low pass filter with corner frequency of 20 Hz and a high pass acausal Butterworth filter with a corner frequency of 0.025 Hz and a filter order of 2 are used for processing the accelerations with and without pads.

number of periods. Filter orders of 4 and 5 are compared by Bazurro *et al.* (2004) up to 10 s and similar results to this study have been obtained.

Response spectra are compared for the noise-free simulated accelerogram acausally filtered with and without pads in Fig. 20. It is apparent that up to 25 s, there is no difference between data filtered with and without pads. However, after 25 s, only the response spectra obtained from the padded data approaches the noise-free response spectra obtained from the simulated accelerogram. The response spectra obtained from pad stripped data show spurious amplified low-frequency spectral amplitudes that should essentially be non-existent for high pass filtered data. The spectra obtained from data without pads predicts substantially higher displacement demand for long periods compared to the spectra obtained from the simulated accelerogram or the data with pads. However, it should hereby be stated that this difference is outside the engineering periods of interest and thus, it can be concluded that the response spectra will not be affected much from zero padding for the engineering periods of interest.

A recent statistical study by Bazurro *et al.* (2004) between periods of 0 to 10 s shows that the response spectra are insensitive to the causality of the filters. In the present paper, the response spectra obtained from the causally and acausally filtered data are compared with the spectra obtained from the noise-free simulated accelerogram as shown in Fig. 21 for a 5% damped system and for a period range between 0 to 100 s. It is apparent that up to a period range of 15 s, the response spectra are indeed insensitive to the causality of the filters. The spectra obtained from causal and acausal filters match the spectra obtained from the simulated noise-free accelerogram exactly. After 15 s, there are dissimilarities in the response spectra and especially pronounced differences in the spectral displacement amplitudes. However, the spectra obtained from the acausally filtered data matches the spectra obtained from the unfiltered simulated noise-free accelerogram more closely than the spectra obtained from the causally filtered data for larger periods.
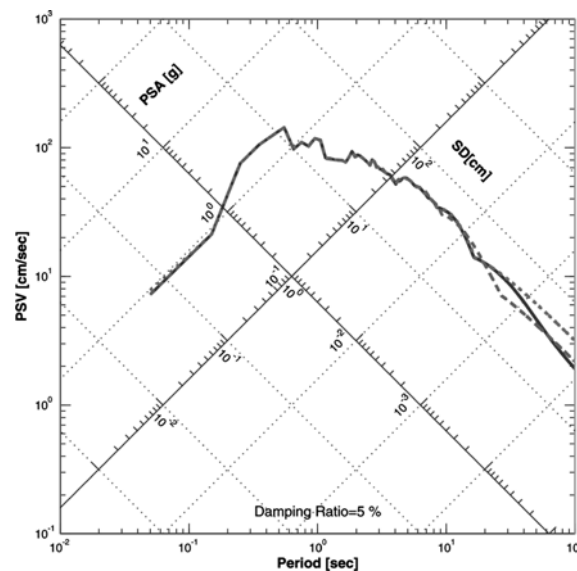

Fig. 21 Response spectra (damping ratio ξ = 5%) for the noise-free unfiltered simulated accelerogram (dotted line) and for the noise-free simulated accelerogram filtered with acausal (solid line) and causal filters (dashed line). The filter parameters are a corner frequency of 20 Hz for the low pass causal filter, a corner frequency of 0.025 Hz for the high pass acausal filter and a filter order of 2.
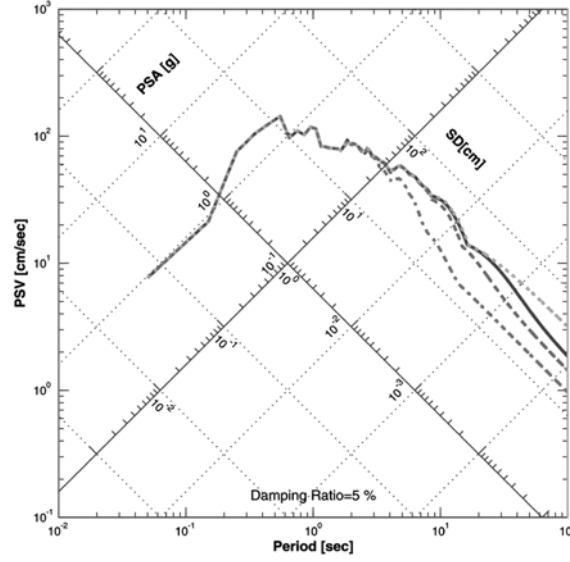
Fig. 22 Response spectra (damping ratio ξ = 5%) for the simulated noise-free accelerogram (dotted line) and noisy simulated accelerogram processed by acausal filters with different corner frequencies: f_c = 0.03 Hz (solid line), f_c = 0.06 Hz (dashed line) and f_c = 0.15 Hz (dashed-dotted line). The low pass filter corner frequency is 20 Hz and the order of the filter is 2.
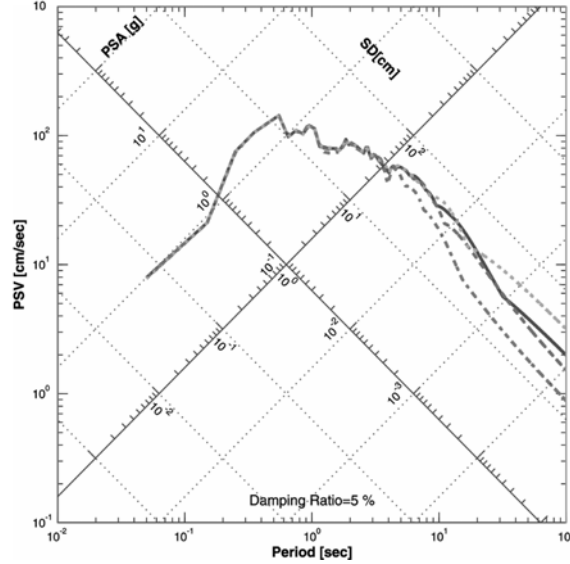

Fig. 23 Response spectra (damping ratio ξ = 5%) for the noise-free simulated accelerogram (dotted line) and the noisy simulated accelerogram processed by causal filters with different corner frequencies: f_c = 0.03 Hz (solid line), f_c = 0.06 Hz (dashed line) and f_c = 0.15 Hz (dashed-dotted line). The low pass filter corner frequency is 20 Hz and the order of the filter is 2.

Fig. 22 shows the response spectra plotted for the noisy simulated accelerogram processed by acausal filters with different corner frequencies. The corner frequency of 0.03 Hz is the only corner

frequency chosen from the review of FAS based on the f^2 source model of Brune. The spectra obtained from the noise free simulated accelerogram are also plotted on the same figure. It is apparent that dissimilarities start after a period of 3 s. Thus, within engineering periods of interest, there are considerable differences between records processed by acausal filters with different corner frequencies both in the spectral velocity and spectral displacement as well as spectral acceleration amplitudes. For long period structures, the displacement demand for the accelerogram filtered with the highest corner frequency is substantially smaller than the accelerogram filtered with lower corner frequencies. Similar conclusions can also be drawn from the noisy simulated accelerogram processed by causal filters with different corner frequencies as shown in Fig. 23. It is apparent that differences in the response spectra arise as low as 1.5 s and considerable differences in the spectral displacements are observable for different corner frequencies. Fig. 22 also shows that the displacement sensitive spectral region for the record processed with a corner frequency of 0.15 Hz is much wider than the record processed with a corner frequency of 0.03 Hz. This has the consequence that the fundamental vibration period of a high rise structure will be in the displacement sensitive region for the record processed with a higher corner frequency whereas it may still be in the velocity sensitive region for the record processed with a lower corner frequency. If a high rise frame building with a fundamental period of 5 s is considered, the first and second higher mode vibration periods will be approximately 1.65 s and 1.0 s (Taghavi and Miranda 2005). Fig. 22 shows that the higher mode contributions would almost be the same for this case regardless of the filter cut-off value. However, for the record filtered by the higher corner frequency, the predicted contribution of the first mode to the response quantities such as base shear would be much less than that of the higher modes.

The supplementary dampers are most effective for structures whose fundamental period is within the velocity sensitive region. The effect of supplementary dampers and displacement demand for high rise structures will be underestimated for the record processed with the higher corner frequency compared to the noise-free response spectra. This is due to the fact that the velocity sensitive region is the narrowest in the spectra obtained from the record with the highest corner frequency.

7. Conclusions

This study examines the influence of causal and acausal filters on the velocity and displacement time history, and the response spectra in comparison with the noise-free results obtained from a simulated accelerogram. The parametric studies show that there are considerable phase distortions in the displacements obtained by causal filters. It is also apparent that the response spectra from the acausal filters match the spectra obtained from the simulated accelerogram more closely than the spectra from causal filters. It is clearly evident from this study that in terms of the structural response, the acausal filters are preferable to the causal filters. The order of the Butterworth filters and the method of integration (whether analtytical integration from a spline fit or numerical integration) do not have any influence on the velocity and displacement waveforms as well as the response spectra. The response spectra at long periods are mostly influenced by the inclusion of pads. However, for the engineering periods of interest, the spectra obtained from the pad stripped data would not differ much from the padded data.

One of the most important parameters influencing the response spectra is the corner frequency. In this study, it is shown that the f^2 model of Brune should be strictly obeyed at low frequencies when

choosing the filter corner frequency from the FAS. If the high pass filter corner frequency is selected according to this rule, the differences between the noise-free spectra obtained from the simulated accelerogram and the spectra obtained from filters, whether causal or acausal, remain small for a great range of periods. This means that caution is required in the review of the FAS. It should also be stated that the corner frequency selection should be made component by component and the same corner frequency should not be used for processing all of the components of a strong-motion record.

The damage measures such as strong-motion duration, Housner spectral intensity, HUSID plots, ARIAS intensity and power of strong-motion are independent of the causality of the filters and also independent of the corner frequency.

The incorrect choice of the corner frequency has also important implications for engineering structures. If the corner frequency of high pass filters is chosen too high, this will result in a narrower velocity sensitive region and consequently the underestimation of the beneficial influence of additional dampers as a rehabilitation choice for the existing high rise buildings. The relative contribution of higher modes to the base shear will also be overestimated as the spectral acceleration corresponding to the fundamental period will be underestimated.

The most adverse effect of using high pass filters is the removal of the SRD which is important for structures traversing active faults such as bridges or viaducts. The disagreement among the earthquake engineering community is today focused on the causality of the filters, whether the accelerogram is obtained from the near-fault or far-fault records. This study shows that, for far-fault records (recorded at a distance greater than 20 km to the surface projection of the fault), the acausal filters are clearly preferable to causal filters and can be reliably used in processing accelerograms within the engineering periods of interest. However for records recorded within 20 km to the surface projection of the fault, the authors are of the opinion that the actual question could be whether we should use traditional filters at all for processing near-fault strong ground-motions due to their removal of SRD. It is apparent that new processing methods which accurately model the static residual displacements should be developed for processing near-fault ground motions.

Acknowledgments

References

Bakir, P.G. (2004), "Proposal for a national mitigation strategy against earthquakes in Turkey", *Natural Hazards*, **33**(3), 405-425.
Bakir, P.G. and Boduroglu, H.M. (2002a), "Earthquake risk and hazard mitigation in Turkey", *Earthq. Spectra*, **18**(3), 427-447.
Bakir, P.G. and Boduroglu, H.M. (2002b), "Mitigating against earthquakes in Turkey", In *Twelfth European Conf.*

on Earthquake Engineering, Barbican Center, London, September.

Bakir, P.G. and Boduroglu, H.M. (2004), "A comprehensive model for earthquake risk reduction in Turkey", In *13th World Conf. on Earthquake Engineering*, Vancouver, Canada, August.

Boore, D.M. (2005a), "On pads and filters: Processing strong-motion data", *Bulletin of the Seismological Society of America*, **95**(2), 745-750, April.

Boore, D.M. (2005b), Personal Communications.

Boore, D.M. and Akkar, S. (2003), "Effect of causal and anti-causal filters on elastic and inelastic response spectra", *Earthq. Eng. Struct. Dyn.*, **32**(11), 1729-1748.

Boore, D.M. and Bommer, J.J. (2005), "Processing of strong-motion accelerograms: Needs, options and consequences", *Soil Dyn. Earthq. Eng.*, **25**(2), 93-115.

Boore, D.M., Stephens, C.D. and Joyner, W.B. (2002), "Comments on baseline correction of digital strong-motion data: Examples from the 1999, Hector Mine California earthquake", *Bulletin of the Seismological Society of America*, **92**(4), 1543-1560.

Brady, A.G. and Trifunac, M.D. (1975), "A study on the duration of strong earthquake ground motion", *Bulletin of Seismological Society of America*, **65**, 581-626.

Bray, J.D. and Rodriguez-Marek, A. (2004), "Characterisation of forward directivity ground motions in the near-fault regions", *Soil Dyn. Earthq. Eng.*, **24**, 815-828.

Brune, J.N. (1970), "Tectonic stress and the spectra of seismic shear waves from earthquakes", *J. Geophysical Research*, 75.

Brune, J.N. (1971), Correction. *Journal of Geophysical Research*, **76**, 5002.

Chopra, A.K. (2001), *Dynamics of Structures: Theory and Applications to Earthquake Engineering*. 2nd edition. Prentice Hall, Upper Saddle River, NJ.

Converse, A.M. and Brady, A.G. (1992), *BAP: Basic Strong-motion Accelerogram Processing Software, Version 1.0*. Open-File report 92-296A, U.S. Department of the Interior U.S. Geological Survey, Middlefield Rd. Menlo Park, CA, 94025.

Housner, G.W. (1952), "Intensity of ground motion during strong earthquake", Earthquake Research Laboratory, California Institute of Technology, Pasadena, California.

Jackson, L.B. (1991), *Signals, Systems, and Transforms*. Addison-Wesley, Univ.of Southern California.

Kanasewich, E.R. (1981), *Time Sequence Analysis in Geophysics*. The University of Alberta Press.

Kiremidjian, A.S. and Singhal, A. (1996), "A method for earthquake motion-damage relationships with application to reinforced concrete frames", Blume Earthquake Engineering Center, Department of Civil and Environmental Engineering, Stanford University-Report No:119, Stanford CA 94305-4020.

Luco, N., Silva, W., Bazzurro, P., Sjoberg, B. and Darragh, R. (2004), "Effects of strong motion processing procedures on time histories, elastic and inelastic spectra", In *Invited Workshop on Strong-motion Record Processing*, The Consortium of Organizations for Strong-Motion Observation Systems (COSMOS), May.

MATLAB 7.0. (2005), The Mathworks Inc. http://www.mathworks.com.

Mitra, S.K. (2001), *Digital Signal Processing*, McGraw-Hill, Second Edition.

Mulholland, R.J., Pitstick, G.M. and Cruz, J.R. (1986), "Approximate realization algorithms for truncated impulse response data", *IEEE Trans. Acoust., Speech, Signal Processing*, **34**, 1583-1588.

Newmark, N.M. and Hall, W.J. (1982), *Earthquake Spectra and Design*. Earthquake Engineering Research Institute Monograph Series.

Nigam, N.C. and Jennings, P.C. (1968), "Digital calculation of response spectra from strong motion earthquake records", CALTECH, Report, Pasadena, California..

Park, S.W., Ghasemi, H., Shen, J., Somerville, P.G., Yen, W.P. and Yashinsky, M. (2004), "Simulation of the seismic performance of the Bolu viaduct subjected to near-fault ground motions", *Earthq. Eng. Struct. Dyn.*, **33**, 1249-1270.

Priestley, M.J.N. and Calvi, G.M. (2002), "Strategies for repair and seismic upgrading of Bolu viaduct 1, Turkey", *J. Earthq. Eng.*, **6**(Special Issue 1), 157-184.

Somerville, P.G., Smith, N.F., Graves, R.W. and Abrahamson, N.A. (1997), "Modification of empirical strong ground motion attenuation relations to include the amplitude and duration effects of rupture directivity", *Seismological Research Letters*, **68**(1), 199-222.

Stephens, C.D. and Boore, D.M. (2004), "ANSS/NSMP strong-motion record processing and procedures", In

Invited Workshop on Strong-motion Record Processing, COSMOS, May.

Taghavi, S. and Miranda, E. (2005), "Approximate floor acceleration demands in multistorey buildings. I: formulation", *J. Struct. Eng.,* ASCE, **131**(2), 203-211.

Vaccaro, R.J. (1983), "Approximate realization and model reduction for linear systems", Ph.D. Dissertation, Department of Electrical Engineering, Princeton University.

Vaccaro, R.J. (2005), *Lecture Notes on 'Subspace Based Signal Processing'.* Graduate School in Systems and Control, Katholieke Universiteit Leuven, Belgium.